Chalcogenide Letters Vol. 7, No. 3, March 2010, p. 203 - 209

EPR AND OPTICAL STUDIES OF ZnS: Mn NANOPARTICLES

R. KRIPAL*, A. KUMAR GUPTA
EPR Lab., Department of Physics, University of Allahabad, Allahabad-211002 India.

Mn-doped ZnS nanoparticles are prepared by chemical method without using any extra capping agent. The electronic structure of Mn-doped ZnS nanoparticles is studied with electron paramagnetic resonance (EPR). The size of the particle is determined by X-Ray line broadening. The average size of primary crystallite nanoparticle was found to be ~ 2 nm. UV-Visible optical absorption study is used to determine the optical band gap of the nanocrystalline. The photoluminescence and EPR spectra of the sample confirm the incorporation of Mn^{2+} in ZnS nanocrystals. The spectroscopic splitting factor of the sample g = 2.0270, the hyperfine splitting constant $A=60\times10^{-4}cm^{-1}$and the crystal field strength $D= 66\times10^{-4}cm^{-1}$.

(Received February 25, 2010; accepted March 1, 2010)

Keywords: Nanocrystal, Capping agent, Photoluminescence, XRD

1. Introduction

Doped semiconductors have been studied extensively in past few decades [1-4]. The interest in doped semiconductors is mainly due to their luminescence properties. Both photoluminescence and electroluminescence at different wavelengths could be achieved upon doping different ions in the same host semiconductors. The optical properties can be tuned due to quantum-size effects, which effectively lead to a size-dependent variation of the band gap energy [5-9]. The greater overlap between the host and dopant wave functions in a nanocrystal compared to the bulk material leads to an enhancement of luminescence intensity due to increased transfer of energy between the host and dopant levels. It is also claimed that the increase in this overlap leads to a drastic reduction of the radiative lifetime of the Mn orange emission [10]. Since the surface energy of the nanoparticles is very high, agglomeration takes place and particle size increases. To avoid this agglomeration many researchers have used capping agents or surfactants but it is very difficult to completely washout the capping agents or surfactants. Thus, unwanted defect layers could be introduced in the NPs. Therefore, a technique is preferred that does not use any external capping agent. In the present work, we have studied the effect of doping of Mn in ZnS nanocrystal without using any external capping agent. The sample characterization is carried out using X-ray diffraction (XRD), transmission electron microscopy (TEM), UV-Visible spectroscopy, photoluminescence (PL) and electron paramagnetic resonance (EPR) techniques.

2. Experimental

For the sample preparation we take manganese acetate [Mn $(CH_3COO)_2$ $4H_2O$], zinc acetate [Zn $(CH_3COO)_2.2H_2O$] and sodium sulfide [Na_2S]. All the chemicals are of AR grade and purchased from Merck. Manganese doped ZnS nanocrystals were prepared by simple chemical route in aqueous medium. 10ml of 1.0 M zinc acetate solution was diluted to 80 ml with the help of distilled water and 10 ml of 0.1 M manganese acetate solution was added drop wise, which was

* Corresponding author: ram_kripal2001@rediffmail.com

followed by drop wise addition of 10 ml of 1 M of Na_2S under vigorous stirring. The pH of the solution was 13.5. In this process Ostwald ripening takes place. A white precipitate was obtained which was separated by centrifugation. The precipitate was washed several times with double distilled water and ethanol. The precipitate was then dried under vacuum at 60 ^{0}C to get the powdered sample.

3. Results and discussion

Fig. 1(a) shows the wide-angle X-ray diffraction patterns of Mn-doped and undoped ZnS NPs at room temperature. The obtained peak positions (111), (220) and (311) correspond to the Bragg angles 28.5°, 47.7° and 56.5° and were very broad which show the zinc blend structure of the sample.

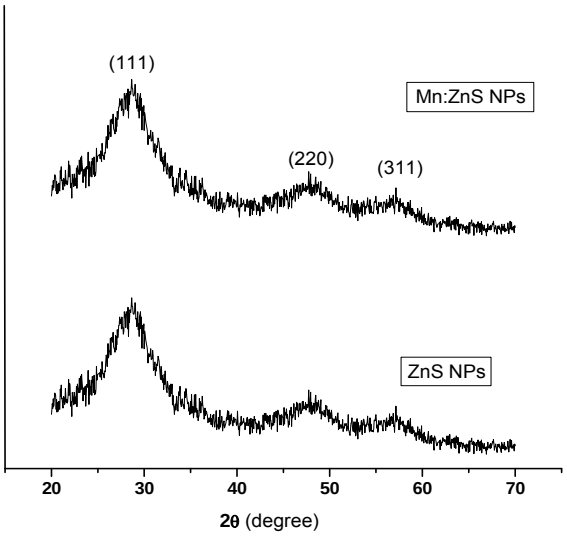

Fig.1 (a).Wide angle XRD Pattern of Mn: ZnS Nanoparticles at room temperature.

The Scherer formula [11] is given by

$$L = [0.9\lambda]/ \beta Cos\theta$$

where L is the coherence length, β is full width at half maximum (in radian) of the XRD peaks, θ is the diffraction angle and λ is the wavelength of X-ray used. The diameter of crystallite is given by

$$D = (4/3)\ L$$

The primary crystallites size using Scherer formula is about 2 nm. TEM image of Mn doped ZnS NPs is shown in the Fig.1 (b). TEM image shows about 20 nm grain size of the Mn doped ZnS NPs. The difference between XRD and TEM data may be due to: (1) there may be more than one crystallite in single grain; (2) there may be some agglomeration of the particles. TEM image also confirms that the particles are highly arrested by the free acetate ions, which are working as a capping agent. When zinc acetate and manganese acetate are dissolved in water, they dissociate into corresponding Zn^{2+}, Mn^{2+} and CH_3COO^{2-} ions. Similarly Na_2S dissociate into Na^+ and S^{2-} ions. The Mn doped ZnS NPs nucleate by consuming more Zn^{2+}, S^{2-} and Mn^{2+} ions from the solution while Na^+ ions accumulate to form the stern layer over Mn doped ZnS NPs, attracting acetate ions to form a diffused layer over it. In this way the particle growth is stopped. The SAED pattern in Fig. 1 (c) shows the diffused rings pattern due to capping discussed above.

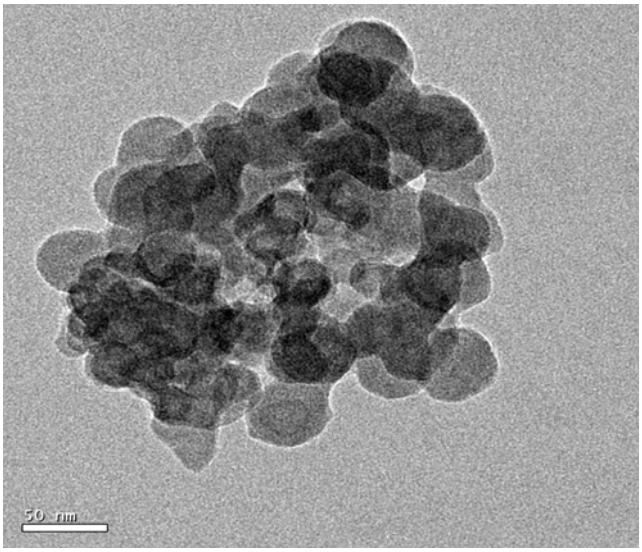

Fig. 1(b) TEM image of Mn:ZnS Nanoparticles.

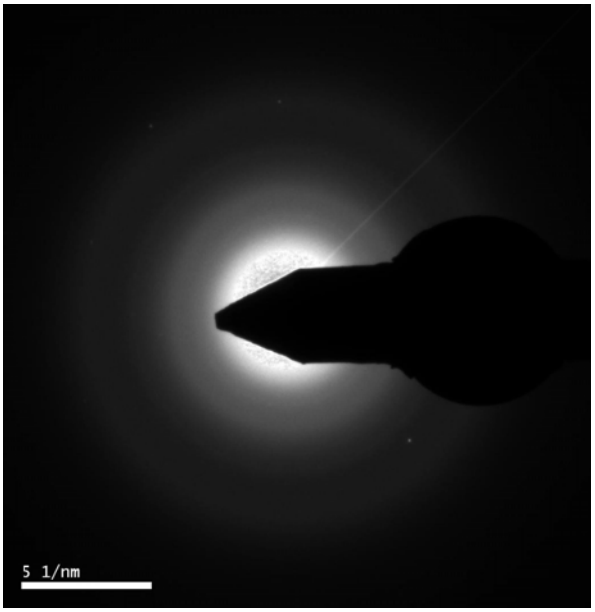

Fig. 1(c) SAED pattern of Mn: ZnS nanoparticles.

The UV-Visible absorption spectrum of the sample in Fig. 2 shows the maximum absorption of doped and undoped ZnS NPs at 306 and 305 nm, respectively, which gives the optical energy band gap of the order of 4.06 and 4.05 eV. These gaps are greater than the value for the bulk sample (3.7eV).This change in band gap may be attributed to confinement effects due to the nanostructure of the ZnS: Mn. Bhargava et. al. [10] suggested that with decreasing particle size a strong hybridization of the s-p states of the ZnS host and the d states of the Mn^{2+} impurity should occur. This hybridization results in a faster energy transfer between the ZnS host and Mn^{2+} impurity yielding higher quantum efficiency.

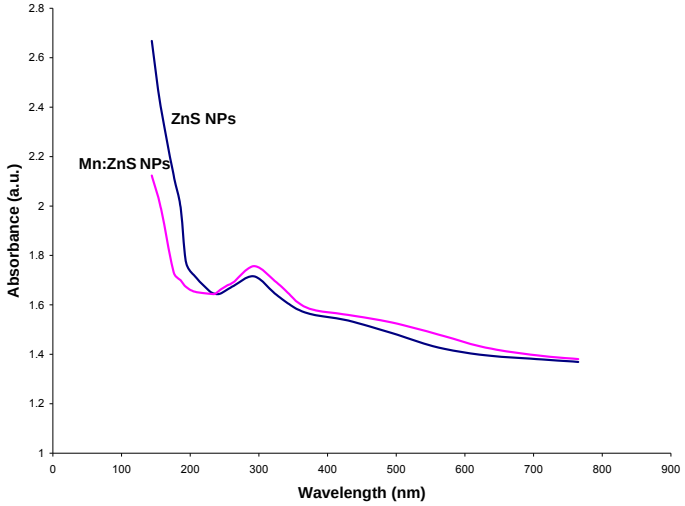

Fig. 2 Absorption Spectrum of ZnS:Mn at room temperature.

In Fig.3 shows the photoluminescence spectra of ZnS: Mn nanoparticle at room temperature. Due to the 325 nm excitation wavelength the orange emission peak is observed at about 587 nm. This emission is possible due to $^4T_1$ to $^6A_1$ transition of Mn^{2+} ions [12] and confirms the doping of Mn^{2+} ions in ZnS nanocrystals.The blue green emissions centered at 417, 443, 479 and 522 nm arise due to interstitial sulfur (I_S) lattice defects, interstitial zinc (I_{Zn}) lattice defect, sulfur vacancies (V_S) and zinc vacancies (V_{Zn}), respectively [13-19]. These are self activated emission bands in ZnS NPs. Since sulfur ions have larger ionic radii (1.7 Å) than that of zinc ions (0.67 Å), interstitial sulfur produces more strain in the ZnS lattice and thus the electron levels due to this site will have smaller binding energy. Therefore interstitial sulfur energy levels must be closer to valence band than the interstitial zinc energy levels to the conduction band. Similarly sulfur vacancy states are closer to conduction band edge than zinc vacancy states to the valence band edge. Hence the peak at 417 nm is assigned to interstitial sulfur, 443 nm is assigned to interstitial zinc, 479 nm to sulfur vacancy and 522 nm to zinc vacancy defect states [20]. The peak at 356 nm originated due to band edge transition.

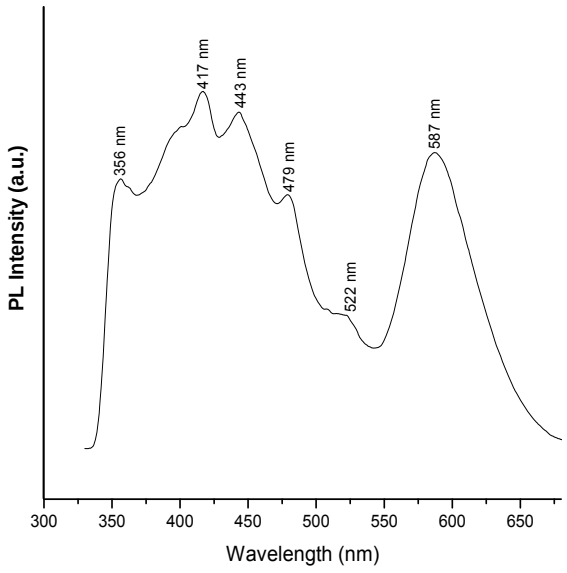

Fig. 3 Photoluminescence Spectra of ZnS: Mn Nanoparticles at room temperature.

Actually, $^4T_1$ to $^6A_1$ transition is spin forbidden, but the weak spin-orbital interaction makes this transition slightly allowed. Since Mn center contains d^5 electron and all the d-states have even parity, the transition between the energy levels of Mn center is forbidden. But in the presence of crystal field the electric dipole transitions become possible due to the mixing of odd-parity states into the d-states. Due to this mixing a small fraction of 4p atomic orbital is likely to mix into 3d orbital and electric dipole transition between ground state $^6A_1$ (spin 5/2) and first excited state $^4T_1$ (spin 3/2) becomes allowed resulting orange emission [21]. In general, the intensity of orange emission is high as compared to blue green emission in ZnS NPs because of the small mixing of 4p atomic orbital into 3d orbital due to strong capping of particles.

The EPR spectrum of the sample, recorded using a Varian E-112 X-band spectrometer with 100 KHz field modulation and 9.1 GHz microwave frequency, is shown in Fig.5a. The EPR spectrum shows eight-line pattern. For Mn^{2+} there are only six allowed transitions corresponding to $\Delta M_s = \pm 1$ and $\Delta M_I = 0$. The additional two lines appear due to forbidden transitions with $\Delta M_s = \pm 1$ and $\Delta M_I = \pm 1$ or ± 2. In ZnS lattice containing substitutional Mn^{2+}, hyperfine transitions are possible due to $\Delta M_s = \pm 1$ and $\Delta M_I = 0$, that is, $\pm 5/2 \leftrightarrow \pm 3/2$, $\pm 3/2 \leftrightarrow \pm 1/2$ and $+1/2 \leftrightarrow -1/2$ transitions. But the random orientations cancel out the anisotropic contributions from $\pm 5/2 \leftrightarrow \pm 3/2$ and $\pm 3/2 \leftrightarrow \pm 1/2$ transitions. Thus only $+1/2 \leftrightarrow -1/2$ transition shows six line spectrum. The EPR spectrum was simulated using EasySpin [22] and is given in Fig. 5b.The simulated EPR spectrum agrees well with the experimental spectrum.

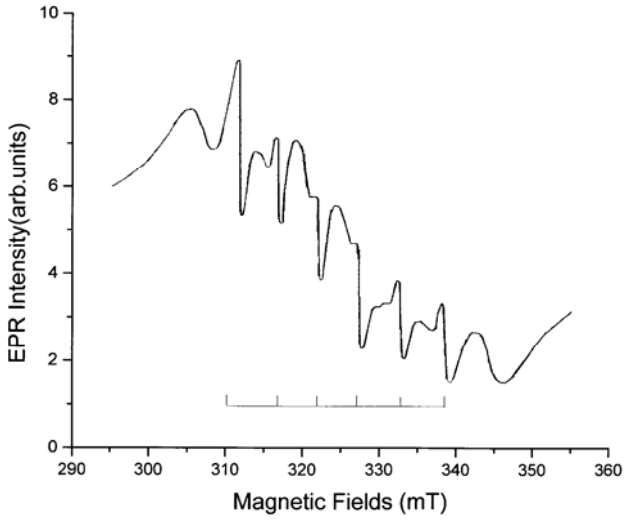

Fig.4 (a) EPR spectra of ZnS: Mn nanoparticlec at room temperature.

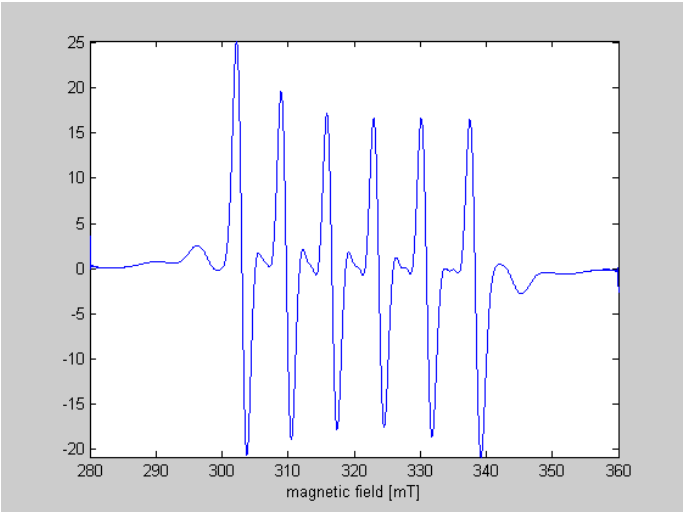

Fig.4 (b) Simulated EPR spectra of ZnS:Mn nanoparticlec at room temperature. (Frequency = 9.1GHz)

The spin Hamiltonian can be written as

$$H = g\mu_B \mathbf{B.S} + A\mathbf{S.I} + (1/6)a(S_x^4 + S_y^4 + S_z^4) + D[S_z^2 - (1/3)S(S+1)]$$

The first term is the Zeeman interaction with isotropic g in the present case. Here μ_B is the Bohr magneton, **B** is the applied magnetic field, g is spectroscopic splitting factor, D is the crystal field strength and A is the hyperfine interaction constant. The second term is the hyperfine interaction with the ^{55}Mn nucleus and leads to a splitting into six lines. The third term is the cubic-field splitting observed in oriented single crystals. The fourth term is the fine-structure splitting.
From EPR spectra, A is calculated as $60\times10^{-4}cm^{-1}$ and D is about $66\times10^{-4}cm^{-1}$ which shows that the doping of Mn^{2+} in ZnS nanocrystals are very small. Thus disorders in the crystal are also small. The Mn-doped ZnS nanocrystals contain various types of disorders, the size of the nanocrystals, the position of Mn within each nanocrystal, aggregation of nanocrystals and differences in surface passivation of each crystal. The EPR experiment detects ensemble average of all these properties. The random distribution of Mn^{2+} ions would obey Poisson statistics. The probability for N centers of Mn^{2+} in a nanocrystal is given as

$$P(N) = (X^N e^{-N})/(N!)$$

where X is the mean number of Mn^{2+} centers per nanocrystals.The distribution of Mn^{2+} ions in doped nanocrystals also depends upon the particle size and surface modification [23].
Igarashi et. al. [24] prepared Mn-doped ZnS nanocrystals by chemical method and found the value of g = 2.0024 and A = $69\times10^{-4}cm^{-1}$ with cubic symmetry of ZnS matrix and tetrahedral site. The value of g and A are sensitive to the coordination state around Mn^{2+}. Borse et. al. [25] also confirm the cubic structure of Mn-doped ZnS nanocrystal on the basis of XRD peaks (111),(220),(311) and EPR parameters g = 2.001, A = $63\times10^{-4}cm^{-1}$, D = $1\times10^{-4}cm^{-1}$ as shown in Table 1. In the present study g = 2.0270, A = $60\times10^{-4}cm^{-1}$ D = $66\times10^{-4}cm^{-1}$and XRD peaks (111), (220), (311) suggest a distorted tetrahedral coordination of the Mn^{2+} within ZnS nanocrystals [25, 26]. The peak-to-peak line widths of EPR lines are about 11G from which we conclude that the Mn^{2+}ions are incorporated within the ZnS and not on the surface of ZnS nanocrystals [25].

Table 1 EPR parameter of sextet lines due to Mn^{+2} substitutionally incorporated in different matrices

Matrix material	Symmetry	Site	g value	A($x10^{-4}$cm)	D($x10^{-4}$cm)	Ref.
ZnS(zinc blende)	cubic	T_d	2.0025	64	0	27
ZnS (zinc blende)	cubic	T_d	2.0064	64	37.4	4
ZnS(wurtzite)	hexagonal	T_d	2.0016	65	105	28
ZnS(zinc blende)	cubic	T_d	2.001	63.9	1	25
ZnS(zinc blende)	cubic	T_d	2.0024	69	xx	24
ZnS(zinc blend)	cubic	distorted T_d	2.0270	60	66	This work
T_d -Tetrahedral						

The positive shift in g value from free electron value indicates that the electrons are transferred from ligand to metal ion [26].

4. Conclusions

We have prepared Mn^{2+} doped ZnS nanoparticles by chemical method without using any external capping agent. In our sample, acetate ions are free and work as the capping agent. The absorption peak appears at around 306 nm, which is fairly blue-shifted from the absorption edge of the bulk. The EPR spectra conclude that our sample has distorted tetrahedral coordination. There is a positive shift in g value from free electron value which indicates that the electrons are transferred

from ligand to metal ion. The order of hyperfine splitting constant confirms that Mn^{2+} ions are incorporated within the ZnS nanocrystals.

Acknowledgement

The authors are very greatful to Prof. A.K. Gupta NCEMP, Allahabad, India for providing XRD facility and Prof. A.C. Pandey, Nanophosphor Application Center University of Allahabad, Allahabad, India, for providing TEM and PL facility. The author Atul Kumar Gupta is also thankful to U.G.C. for providing Junior Research Fellowship.

References

[1] H. C. Ong, R. P. H. Chang, Appl. Phys. Lett. 79 3612 (2001).
[2] Y. C. Fang, S. Y. Chu, H. C. Chen, J. Electrochem. Soc **156** k55 (2009).
[3] S. Kar, S. Biswas, J. Phys. Chem. C **112** 11144 (2008).
[4] A. Pedro, G. Beermann, R. Bruce, M. Garvey, S. Murlidharan, R.C.W. Sung, Chem. Mater **16**, 917 (2004).
[5] L.E. Brus, J. Chem. Phys. **80**, 4403 (1984)
[6] A.N. Goldstein, C.M. Echer, A.P. Alivisatots, Science **356**, 1425 (1992)
[7] J. Nanda, Sameer Sapra, and D.D. Sarma, Chem. Mater. **12**, 1018 (2000)
[8] R.N. Bhargava, D. Gallagher, X. Hong, and A. Nurmikko, Phys. Rev. Lett.**72**, 416 (1994).
[9] Y.S.Yuang, Y.F.Chen, Y.Y. Lee, L.C.Liu, Japan.J. Appl. Phys.**76**, 3041 (1994)
[10] T.A. Kennedy, E.R. Glaser, P.B. Klein, and R.N. Bhargava, Phys. Rev. B **52**, R14 356 (1995)
[11] D. Xu, G. Guo, L. Gui, Y. Tang, Z. Shi, Z. Jin, Z. Gu, W. Liu, X. Li, G. Zhang, Appl. Phys. Lett.**75**, 481 (1999)
[12] W. Chen, R. Sammynaiken, R.Wallenberg, J.Bovin, J. Appl. Phys. **89**, 1120 (2001)
[13] W. G. Becker, A. J. Bard, J. Phys. Chem. **87** 4888 (1983).
[14] R. N. Bhargava, J. Lumin. **70** 85 (1996).
[15] N. Karar, F, Singh, B. R. Mehta, J. Appl. Phys. **95** 656 (2004).
[16] S. Sapra, A. Prakash, A. Ghanrekar, N. Periasamy, D. D. Sharma, J. Phys. Chem. **109** 1663 (2005).
[17] K. Manzoor, S. R. Vadera, N. Kumar, T. R. N. Kutty, Mater. Chem. Phys. **82**, 718 (2003).
[18] R. Sarkar, C. S. Tiwary, P. Kumbhakar, S. Basu, A. K. Mitra, Physics E **40** 3115 (2008).
[19] A. Singh, M. Limaye, S. Singh, N. P. Lalla, C. K. Malek, S. Kulkarni, Nanotechnology **19** 245613 (2008).
[20] D. Denzler, M. Olschewski, K. Sattler, J. Appl. Phys. **84** 2841(1998).
[21] N.Q.Huong, J.L.Birman, Phys.Rev.B **69**, 085321 (2004).
[22] S. Stoll, and A. Schweiger, J. Magn. Reson. **170**, 42 (2006).
[23] L. Levy, N. Feltin, D. Ingert and M.P. Pileni, J. Phys. Chem. B **101**, 9153 (1997)
[24] T. Igarashi, T. Isobe and M. Senna, Phys. Rev. B, **56**, 11, (1997).
[25] P.H. Borse, D. Srinivas, R. F. Shinde, S.K. Date, W. Vogel, S.K. Kulkarni,. Phys.Rev.B **60**, 8659 (1999).
[26] Electron Paramagnetic Resonance of Transition ions by A. Abragam and B. Bleany.
[27] G.W. Ludwig and H.H. Woodboury, in Solid State Physics, (Academic, New York, 1962), Vol.**13**, p.223.
[28] S.P.Keller, I.L. Gelles, and W.V. Smith, Phys. Rev. **110**, 850 (1958)